


Theory for coherent control of longitudinal optical phonons in GaAs using polarized optical pulses with relative phase locking

Itsuki Takagi ^{1,2}, Yosuke Kayanuma,^{1,3,*} and Kazutaka G. Nakamura^{1,2,†}

¹Laboratory for Materials and Structures, Institute of Innovative Research, Tokyo Institute of Technology, 4259 Nagatsuta, Yokohama 226-8503, Japan

²Department of Materials Science, Tokyo Institute of Technology, 4259 Nagatsuta, Yokohama 226-8503, Japan

³Graduate School of Sciences, Osaka Prefecture University, 1-1 Gakuen-cho, Sakai, Osaka 599-8531, Japan



(Received 15 March 2021; revised 16 September 2021; accepted 20 September 2021; published 1 October 2021)

A theoretical model for the coherent control of longitudinal optical phonons in GaAs (001) by double-pulse excitation was derived using a simplified band model and the allowed and forbidden Raman scattering. The time evolution of the electron-phonon states was calculated with the density-matrix formalism and second-order perturbation. The amplitude of the longitudinal optical phonons controlled by the two pulses was obtained as a function of the delay between the pulses for several polarization conditions. For parallel-polarized pulses, electronic and phonon interference fringes were predicted, which were independent of the crystal orientation and the ratio between the allowed and forbidden Raman scattering intensities. For orthogonally polarized pulses, only phonon interference fringes were obtained at an angle of $\pi/4$ from the [100] direction. When one of the pulses was along the [100] direction, electronic interference fringes were induced by the allowed Raman scattering, although the pump pulses do not interfere themselves.

DOI: [10.1103/PhysRevB.104.134301](https://doi.org/10.1103/PhysRevB.104.134301)

I. INTRODUCTION

Coherent control is the technique of manipulating quantum states in materials using optical pulses [1–3]. This is widely used to manipulate electronic, vibrational, and rotational states of atoms and molecules [4–8], and excitons, spins, and phonons in the solid state [9–15]. Optical phonons can be coherently excited and monitored using ultrashort optical pulses via transient reflectivity or transmissivity using a pump-and-probe technique [16–21]. In this technique, the amplitude of the phonons is controlled using a train of optical pulses or a pulse-shaping technique [22–26] via constructive or destructive interference between the induced phonons. Furthermore, by applying a relative phase of the optical pulses to solid materials, not only phonon interference but also electronic interference can be observed via a quantum-path interference [27].

In our previous works we investigated the coherent control of longitudinal optical (LO) phonons in an *n*-type GaAs single crystal with a (001) surface using relative phase-locked femtosecond double pulses under parallel and perpendicular polarization [27,28]. Using parallel-polarized pump pulses, we observed fine interference fringes of electronic coherence with fast oscillations as well as phonon interference for a longer time than for the optical interference between pump pulses [27]. The generation paths were distinguished from the interference fringe patterns. By contrast, for perpendicularly polarized pump pulses, only phonon interference was observed [28]. This polarization effect can be qualitatively explained using a quantum-mechanical model.

Coherent phonons in GaAs have been widely studied [17,19,23,29,30]. There are two processes that contribute to the generation of LO phonons in GaAs in the opaque regime. The main process for generating LO phonons in GaAs (especially for *n*-doped and *p*-doped samples) is considered to be the transient depletion field screening [19], which is a type of space charge field-induced process. The initial field distribution is suppressed by the opposite drift of the optically induced electrons and holes, and the accompanying depolarization field acts as the nonlinear driving term for the coherent phonons [17]. A stimulated Raman process is another generation mechanism which is different from the transient depletion field screening process and is also discussed to contribute for nondoped GaAs [30].

The stimulated Raman process also includes two interactions. One is a short-range interaction, which is induced by the deformation-potential interaction, and the other is a long-range interaction, such as the Fröhlich interaction [29,30]. The creation and annihilation of phonons by light scattering via the short-range interaction is expressed with dipole-allowed components in a Raman tensor. An ultrashort optical pulse can induce impulsive stimulated Raman scattering (ISRS) to generate optical phonons. Furthermore, the long-range interaction can be treated as the dipole-forbidden components in the Raman tensor [30,31]. The dipole-allowed Raman tensor for LO phonon scattering in a zinc-blende crystal with the (001) surface is an off-diagonal tensor. Then, the electronic polarization rotates with an angle of $\pi/2$ during phonon generation. This suggests an interesting possibility that the electronic states interact with light pulses differently depending on the polarization direction. It would be possible to detect this Raman-induced rotation of the electronic polarization through the ultrafast interferometric pump-probe measurements with

*Corresponding author: kayanuma.y.aa@m.titech.ac.jp

†Corresponding author: nakamura@msl.titech.ac.jp

polarization- and delay-controlled double pulses. On the other hand, for the transient depletion field screening process, the field is perpendicular to the surface and an isotropic polarization dependence for generation of the LO phonons is reported [17,29].

Theoretical calculations for the generation and detection of coherent excited phonons have been performed using several models, in which the lattice oscillation is treated classically or quantum mechanically [16,18,19,32–38]. Recently we developed a quantum-mechanical model with classical optical fields for the coherent control of the amplitude of optical phonons induced by two pulses and applied this to GaAs and diamond crystals [27,28,39]. In these previous works, the effects of polarization correlation between the two pump pulses was not studied in sufficient detail. Thus, in the present work, we focus our attention on the problem of the polarization effects of relative-phase-locked double pulses. As a first step in this direction, we study theoretically the quantum mechanical aspects of the interference fringes for the polarization- and delay-controlled double-pulse excitation of coherent phonons. For the sake of concreteness, we study the coherent control of LO phonons in a GaAs crystal with the (001) surface, using a simplified band model and a total Raman tensor that includes the allowed and forbidden components. The allowed and forbidden Raman components coexist in GaAs and their relative contribution can be controlled by the doping rate. This makes GaAs an interesting test material to evaluate the effects of quantum-path interference. We calculate the amplitude of the LO phonons and quantitatively discuss the phonon and electronic interference behaviors depending on the polarization angles of the pump pulses.

II. MODEL

A. Hamiltonian

We consider the generation of the LO phonons, which propagate along the z axis in a GaAs crystal with a (001) surface upon irradiation of two pump pulses that also propagate along the z axis; we identify the [001] axis as the z axis. The electronic states are assumed to be the electronic ground state ($|g\rangle$) and the two-excited-state bands ($|e_x, k\rangle$, and $|e_y, k\rangle$), which are polarized along the x and y axes, respectively, with the wave number k and are degenerate in energy. We set the x axis along the [100] crystal axis and the y axis along the [010] axis. We use a single-electron approximation in the model. The Hamiltonian of the electron-phonon coupled states is given by

$$H = H_e + H_L + H_{eL}, \quad (1)$$

$$H_e = \varepsilon_g |g\rangle \langle g| + \sum_k \varepsilon_k (|e_x, k\rangle \langle e_x, k| + |e_y, k\rangle \langle e_y, k|), \quad (2)$$

$$H_L = \hbar\omega b^\dagger b, \quad (3)$$

$$H_{eL} = \alpha \hbar\omega \sum_k (|e_x, k\rangle \langle e_y, k| + |e_y, k\rangle \langle e_x, k|)(b^\dagger + b) + \beta \hbar\omega \sum_k (|e_x, k\rangle \langle e_x, k| + |e_y, k\rangle \langle e_y, k|)(b^\dagger + b), \quad (4)$$

where ω is the phonon frequency, and $\varepsilon_g, \varepsilon_k$ are the energies of the ground and excited levels, respectively [28]. The operators b^\dagger, b are the creation and annihilation operators for LO phonons at the Γ point, respectively. In the electron-phonon Hamiltonian H_{eL} , the terms proportional to α and β represent the respective interactions for allowed and forbidden Raman scattering, and the total Raman tensor for LO phonons in GaAs is given by

$$R = \begin{pmatrix} R_\beta & R_\alpha & 0 \\ R_\alpha & R_\beta & 0 \\ 0 & 0 & R_\beta \end{pmatrix}, \quad (5)$$

where R_α and R_β are the polarization rates of the allowed and forbidden Raman scattering, respectively [31,40]. When the light propagates along the z axis, only the $xx, yy, xy,$ and yx planes are relevant. The allowed Raman scattering is due to the deformation-potential interaction, and the forbidden Raman scattering is due to the intraband Fröhlich and Franz-Keldysh [30]. The values α and β are proportional to R_α and R_β , respectively.

Within the rotating-wave approximation, the interaction Hamiltonian between light and electrons is expressed by

$$H_I = E_1(t) \sum_k (\mu_k |e_1, k\rangle \langle g| e^{-i\Omega_0 t} + \text{H.c.}) + E_2(t) \sum_k (\mu_k |e_2, k\rangle \langle g| e^{-i\Omega_0(t-t_{12})} + \text{H.c.}), \quad (6)$$

in which μ_k is the transition dipole moment, Ω_0 is the frequency of the pump pulse, and t_{12} is the delay between pump pulses 1 and 2. Here H.c. represents the Hermitian conjugate terms, and $|e_1, k\rangle$ and $|e_2, k\rangle$ represent the excited state determined by the polarization of pump pulses 1 and 2, respectively:

$$|e_1, k\rangle = \cos\theta |e_x, k\rangle + \sin\theta |e_y, k\rangle, \quad (7)$$

$$|e_2, k\rangle = \cos(\theta + \varphi) |e_x, k\rangle + \sin(\theta + \varphi) |e_y, k\rangle, \quad (8)$$

where θ is the angle between pump pulse 1 and the x axis, and φ is the relative angle between pump pulses 1 and 2, as shown in Fig. 1. $E_1(t)$ and $E_2(t)$ are the optical electric field of pump pulses 1 and 2, respectively, and are expressed by $E_1(t) = E_0 f(t)$ and $E_2(t) = E_0 f(t - t_{12})$. The function $f(t)$ is the Gaussian pulse envelope, which is defined by

$$f(t) = \frac{1}{\sqrt{\pi}\sigma\Omega_0} \exp\left(-\frac{t^2}{\sigma^2}\right), \quad (9)$$

where E_0 is the amplitude of the electric field and σ is the pulse width.

In this model we consider the process by which coherent phonons are generated under resonant excitation to slightly above the band edge of GaAs. It should be noted that the band gap depends on the temperature [41] as well as on the doping rate [42]. We introduce the effective response function $F(t)$ phenomenologically, which describes the electronic transition rate to the energy region relevant to the resonant Raman scattering. Formally, $F(t)$ is written as

$$F(t) = \sum_k |\mu_k|^2 e^{-\frac{i}{\hbar}(\varepsilon_k - \varepsilon_g)t - \eta|t|/\hbar} \quad (\eta = 0_+), \quad (10)$$

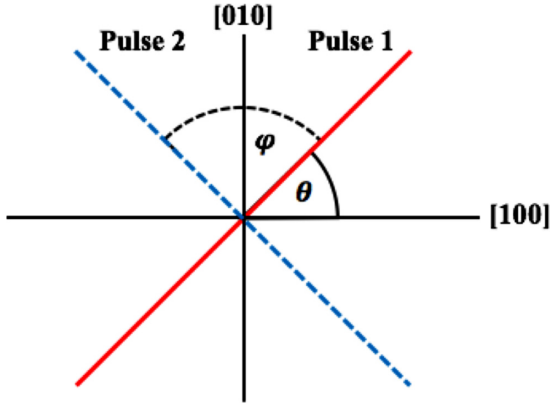


FIG. 1. Electric polarization of pulses 1 and 2 and the crystalline axes [100] and [010], which designate the x and y directions, respectively. θ is the angle between the polarization of pulse 1 and the [100] axis, and φ is the angle between the polarization of pulses 1 and 2.

in which μ_k is the effective transition dipole moment from the ground state to $|e_x, k\rangle$ and $|e_y, k\rangle$ in the excited states. In actual calculations we adopt a simple form,

$$F(t) \propto |\mu|^2 \exp(-i\Omega_c t - \Gamma|t|), \quad (11)$$

where Ω_c is the central frequency and Γ is the electronic phase relaxation rate in the conduction band. The main origin of the phase relaxation is the inhomogeneous width in the conduction band as described by the summation in Eq. (10). The Fourier transformation of Eq. (11) is a Lorentzian function $I_{\text{eff}}(\Omega) = I_0(\Gamma/\pi)/[(\Omega - \Omega_c)^2 + \Gamma^2]$, which corresponds to an effective density of states relevant to ISRS with a center energy of $\hbar\Omega_c$ and a bandwidth of $\hbar\Gamma$.

B. Transition paths for generating phonons via ISRS process

We adopt the density-matrix formalism to derive the generation amplitude of coherent phonons by solving the time-dependent Schrödinger equation with the second-order perturbation. The change of the amplitude ΔR of the reflectivity is proportional to the expectation value of the LO phonon coordinate $Q = \sqrt{\hbar/2\omega}(b + b^\dagger)$.

Figure 2 presents double-sided Feynman diagrams for the generation of LO phonons by ISRS with two pump pulses. The initial state in the ket vector is assumed to be the electronic ground state with the zero-phonon state $|g, 0\rangle = |g\rangle \otimes |0\rangle$, and the final state is $|g, 1\rangle = |g\rangle \otimes |1\rangle$. The kets $|e_1, 0\rangle$, $|e'_1, 1\rangle$, $|e_2, 0\rangle$, $|e'_2, 1\rangle$ denote the electronic excited states induced by pulses 1 and 2 with zero- and one-phonon states, respectively. In Fig. 2, t_1 and t_2 denote the times at which the system interacts with the electric field of the pump pulse, and τ denotes the time at which the phonon is created. Photoexcitation and deexcitation processes occur at t_1 and t_2 , respectively. Phonon creation is assumed to occur at an arbitrary time in the electronic states ($t_1 \leq \tau \leq t_2$). Electronic excitation and deexcitation occur within a pulse in paths 1 and 2, and occur in different pulses in paths 3 and 4. For the ISRS, after interacting with the pump pulses, the final electron-phonon state is $|g, 1\rangle |g, 0\rangle$ or $|g, 0\rangle |g, 1\rangle$. In the phonon-creation process, the polarization of the electronic state changes via the allowed Raman components ($|e_x\rangle \rightarrow |e_y\rangle$)

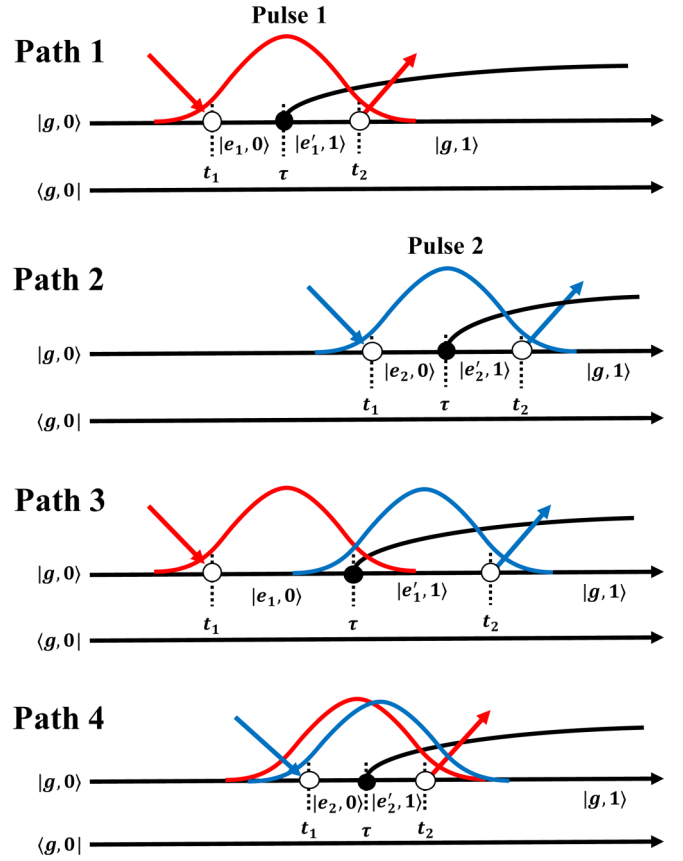


FIG. 2. Double-sided Feynman diagrams for generating LO phonons by pulses 1 and 2. The red and blue curves illustrate the Gaussian shapes of pulses 1 and 2, respectively. The open circles mark the time when electronic excitation and deexcitation are induced by the optical electric field. The solid circle marks the moment when a phonon is generated.

or $|e_y\rangle \rightarrow |e_x\rangle$) but does not change via the forbidden Raman components ($|e_x\rangle \rightarrow |e_x\rangle$ or $|e_y\rangle \rightarrow |e_y\rangle$). When the polarizations of the pulses are taken into account, the amplitude of the LO phonons is expressed by a coherent superposition of the contributions from the allowed and forbidden Raman scattering processes.

The time evolution of the density operator $\rho^{\text{op}}(t)$ is given by the second-order perturbation calculation, and the expectation value of the LO phonon amplitude is expressed by $\text{Tr}[Q\rho^{\text{op}}(t)]$. The relevant part of the density operator $\rho^{\text{op}}(t)$ is written as $\rho^{\text{op}}(t) = \rho(t)|g, 1\rangle\langle g, 0|$ where $\rho(t)$ is expressed by the sum for each transition path $\rho_i(t)$ as

$$\rho(t) = \sum_{i=1}^4 \rho_i(t),$$

as shown in Fig 2. For each path i ($i = 1, 2, 3, 4$), $\rho_i(t)$ is given by

$$\rho_1(t) = (\alpha \sin 2\theta + \beta)P_{11}(t), \quad (12)$$

$$\rho_2(t) = \{\alpha \sin 2(\theta + \varphi) + \beta\}P_{22}(t), \quad (13)$$

$$\rho_3(t) = \{\alpha \sin(2\theta + \varphi) + \beta \cos \varphi\}P_{12}(t), \quad (14)$$

$$\rho_4(t) = \{\alpha \sin(2\theta + \varphi) + \beta \cos \varphi\}P_{21}(t), \quad (15)$$

in which

$$P_{ij}(t) = \left(\frac{E_0}{\hbar}\right)^2 e^{-i\omega t} \sum_k |\mu_k|^2 \int_{-\infty}^t dt_2 \int_{-\infty}^{t_2} dt_1 \times f_i(t_1) f_j^*(t_2) e^{-\frac{i}{\hbar}(\epsilon_k - \hbar\Omega_0)(t_2 - t_1)} \times e^{-\frac{\eta}{\hbar}|t_2 - t_1|} (e^{i\omega t_2} - e^{i\omega t_1}), \quad (16)$$

where ($i, j = 1$ or 2), and the envelope functions are $f_1(t) = f(t)$ and $f_2(t) = f(t - t_{12})e^{i\Omega_0 t_{12}}$. In Eq. (16), t is the observation time, which is much later than the time at which the double pulses are irradiated. Therefore, the upper limit of the integral can be replaced by ∞ . Furthermore, introducing a pair of variables (s, u), which are defined as $s = (t_1 + t_2)/2$, $u = t_2 - t_1$, the integration over s can be carried out. (Details of the calculation are shown in Appendix A.) Thus, we find that $P_{ij}(t)$ is given as a function of the pump-pump delay t_{12} as

$$P_{11}(t) = e^{-i\omega t} L(0), \quad (17)$$

$$P_{22}(t) = e^{-i\omega(t-t_{12})} L(0), \quad (18)$$

$$P_{12}(t) = e^{-i\omega(t-t_{12}/2)} e^{-i\Omega_0 t_{12}} L(t_{12}), \quad (19)$$

$$P_{21}(t) = e^{-i\omega(t-t_{12}/2)} e^{i\Omega_0 t_{12}} L(-t_{12}), \quad (20)$$

except for a common constant factor, and

$$L(x) = 2i \int_0^\infty du e^{-\frac{(u-x)^2}{2\sigma^2}} \sin\left(\frac{\omega u}{2}\right) e^{i\Omega_0 u} F(u). \quad (21)$$

The above formulas are the central results of the present work. They predict that the t_{12} dependence of the phonon amplitude will be composed of two types of quantum-path interference. One is the temporal interference expressed by $P_{ij}(t)$, and the other is the geometrical interference given by the θ and φ dependence in the prefactors of $P_{ij}(t)$. Note that the amplitudes of the ISRS using relative-phase-locked double pulses carry the memory of the phases of the pump pulse by which the electron is excited and deexcited. This is explicitly exhibited in the phase factors in P_{ij} shown in Eqs. (17)–(20). The amplitudes due to paths 1 and 2 do not depend on the phase factor $\Omega_0 t_{12}$, whereas those from paths 3 and 4 carry the factor $\Omega_0 t_{12}$, which is imprinted on the electron coherence. Path 4 may be called an anomalous path, because this term represents the process in which the electron is excited by the *delayed pulse* and deexcited by the *advanced pulse*. Therefore, the contribution from path 4 is limited to the small time-delay region at which the two pulses overlap in the time domain.

C. Transition paths for generating phonons via space-charge field

A vibronic Raman interaction and a surface space-charge field have been discussed as a driving force for coherent phonons in semiconductors. In particular, suppression of a surface space-charge field is the decisive source term for driving the coherent phonons in III-V semiconductors [17]. The initial field distribution is suppressed by the opposite drift of the optically induced electrons and holes, and the

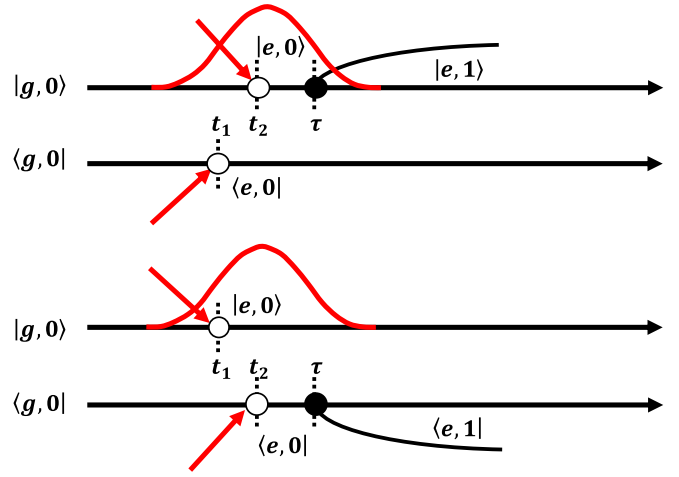


FIG. 3. Double sided Feynman diagrams for generation of coherent phonons via suppression of the surface space-charge field.

accompanying depolarization field acts as the nonlinear driving term for the coherent phonons [17]. According to this mechanism, the driving term depends on an optically induced carrier density \bar{n} , which is obtained by populations in the electronic excited state ($|e, 1\rangle$ $|e, 0\rangle$ and $|e, 0\rangle$ $|e, 1\rangle$) can be expressed as: $|e, 1\rangle \langle e, 0| = [\gamma E_{sc} \hbar \omega \mu_k E_0 f(t) e^{-i\Omega_0 t} |e, 1\rangle \langle g, 0|] \times |g, 0\rangle \langle e, 0|$, where γ is a strength of interaction and E_{sc} is the space-charge field strength.

Figure 3 shows double sided Feynman diagrams of this interaction, in which $t_2 > t_1$. The phonon is created at time τ , at which the electronic transition occurs via the dipole interaction and the population in the electronic excited state is created. The phonon cannot be created by the first interaction at t_1 , which is different from the impulsive absorption case.

The density matrix with the second-order perturbation is obtained as

$$\rho_{ij}(t) = \gamma E_{sc} \left(\frac{E_0}{\hbar}\right)^2 e^{-i\omega t} \sum_k |\mu_k|^2 \times \int_{-\infty}^t dt_2 \int_{-\infty}^{t_2} dt_1 f_i^*(t_1) f_j(t_2) e^{-\frac{i}{\hbar}(\epsilon_k - \hbar\Omega_0)(t_2 - t_1)} \times e^{-\frac{\eta}{\hbar}|t_2 - t_1|} e^{i\omega t_2} |e, 1\rangle \langle e, 0| + \text{H.c.}, \quad (22)$$

where $f_1(t) = f(t)$ and $f_2(t) = f(t - t_{12})e^{i\Omega_0 t_{12}}$. The upper limit (t) of the integral for t_1 and t_2 can be approximately replaced by ∞ for $t \gg t_2$.

III. RESULTS AND DISCUSSION

In the actual calculations we considered a pair of relative-phase-locked femtosecond pulses (pulses 1 and 2) directed along the z axis of the (001) surface of a GaAs crystal.

The width of each pulse was $\sigma = 30$ fs, and the center energy of each pulse was $\hbar\Omega_0 = 1.55$ eV, which is above the band gap (1.52 eV). The frequency of the LO phonons was set to 8.8 THz ($\hbar\omega = 0.036$ eV). The energy of the electronic ground state ε_g was set to zero. For the effective response function $F(t)$, we assumed $\Omega_c = \Omega_0$ and $\Gamma = 0.0455$ (fs) $^{-1}$. This decay constant value corresponds to an energy of 0.03 eV ($\hbar\Gamma = 0.03$ eV). The lifetime corresponding to the decay constant is approximately 22 fs. This may be shorter than the population lifetimes which are measured by using angle-resolved-photoelectron spectroscopy (ARPES) experiments [43,44] (e.g., population lifetime of 165 fs at pump-photon energy of 1.7 eV for *p*-type GaAs (110) [43]). The previous ARPES experiments were not actually measuring the same lifetimes as what is in the present model. This choice of parameter values also reproduced the experimental line shape of the fringe pattern in *n*-GaAs at 90 K for the double-pulse pumping by parallel polarization case [27]. The electronic coherence in the excited state decays with the decay constant Γ (see details in the Appendix B). We could not find a significant shift in an initial coherent-phonon phase due to the lifetime in the previous single-pulse-excitation experiments [27], although the lifetime dependence [45] is predicted for very short pulse excitation. We neglected the decay of phonons in this work.

The values of α and β depend on the doping rate in GaAs. In an intrinsic GaAs, a ratio of $\beta/\alpha = 6$ was used as an example. For *n*-doped GaAs, the allowed Raman scattering is negligible.

In the following parts of this section, we show the general features of the interference fringes in the coherent LO phonon generated by the allowed and forbidden ISRS processes as a function of the angles θ and φ , and the delay t_{12} . For the predictions of the signals expected in real materials, we show results with $\beta/\alpha = 6$ for intrinsic GaAs, and $\alpha = 0$ for *n*-doped GaAs. The amplitude of the LO phonons was obtained by calculating $\text{Tr}[Q\rho(t_{12})]$ with Eqs. (16)–(20) and taking the absolute values. The electronic and phononic interferences were evaluated from a plot of the phonon amplitude as a function of the delay t_{12} between pulses. The calculations show that the interference pattern changes depending on the polarization angle (i.e., θ or φ). The results for the typical polarization conditions are shown in the following subsections.

A. Parallel-polarized pulses ($\varphi = 0$)

Figure 4 shows the calculated amplitude of LO phonons with $\beta/\alpha = 6$ for parallel-polarized pulses with $\varphi = 0$ and $\theta = 0$ as a function of the pulse delay t_{12} . There is a slow oscillation (~ 115 -fs period) owing to phonon interference and a fast oscillation (~ 2.7 -fs period) owing to electronic interference. Under the parallel-polarized condition ($\varphi = 0$), all transition paths have the same factor ($\alpha \sin 2\theta + \beta$) of the effect of the Raman tensor according to Eqs (11)–(14). Then the interference pattern is independent of the values α and β . This means that the interference patterns for intrinsic and *n*-type GaAs are the same. In fact, the interference fringes in Fig. 4 agree well with our previously reported experimental results for *n*-type GaAs (001) [27]. In addition, a change of

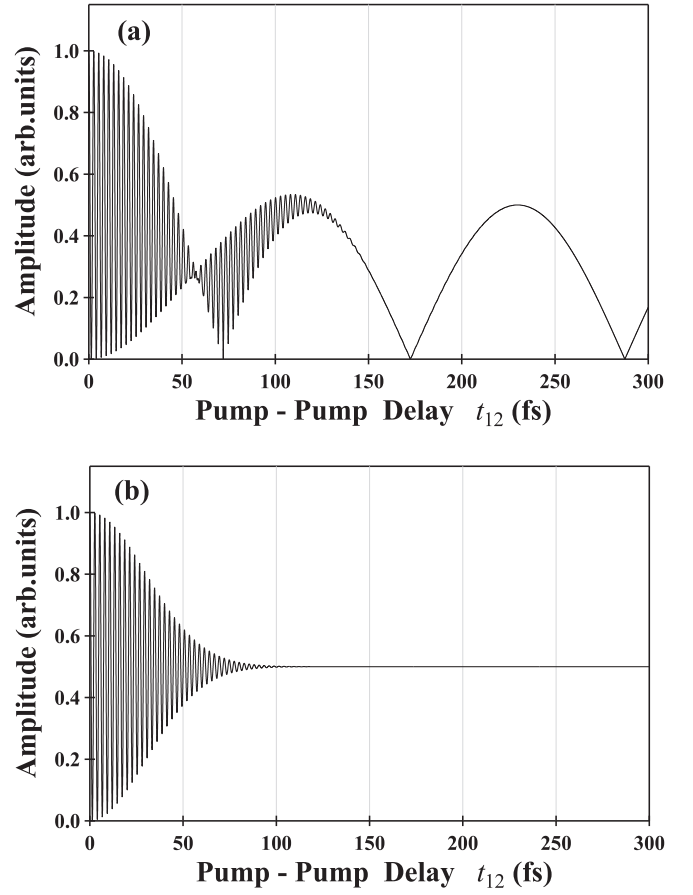


FIG. 4. (a) Amplitude of LO phonons induced by the parallel-polarized pulses ($\theta = 0$) as a function of the pump-pump delay t_{12} . (b) Intensity of optical pulses 1 and 2. The vertical axis is normalized such that the maximum value is 1.

the angle θ , while keeping the relative angle at 0 deg, does not change the interference pattern.

The amplitude of the interference fringes with fast oscillations, which indicate electronic coherence, decreased until approximately 50 fs and thereafter increased (i.e., collapse and revival). Electron coherence is caused by paths 3 and 4. However, path 4 may contribute only at $t_{12} \approx 0$, where the two pulses overlap. At longer time delays, only path 3 contributes to the electronic interference. Then the amplitude of the phonon oscillation is given by the absolute value of $P_{11}(t) + P_{22}(t) + P_{12}(t)$, which is approximately proportional to $|1 + \exp[i\omega_0 t_{12}] + \exp[-i\Omega_0 t_{12}]|$, as can be seen from Eqs. (16)–(18). Note that the rapid oscillation due to the electronic interference appears only through the cross term with the slow component $1 + \exp[i\omega_0 t_{12}]$ of the phonon interference. Therefore, we attribute the collapse and revival of the electronic interference at about $t_{12} \approx 50$ fs is the result of the destructive phonon interference at a half-period.

B. Orthogonally polarized pulses ($\varphi = \pi/2$)

The interference of the LO phonons generated by the orthogonally polarized pulses with $\varphi = \pi/2$ depends on the angle θ (Figs. 5 and 6).

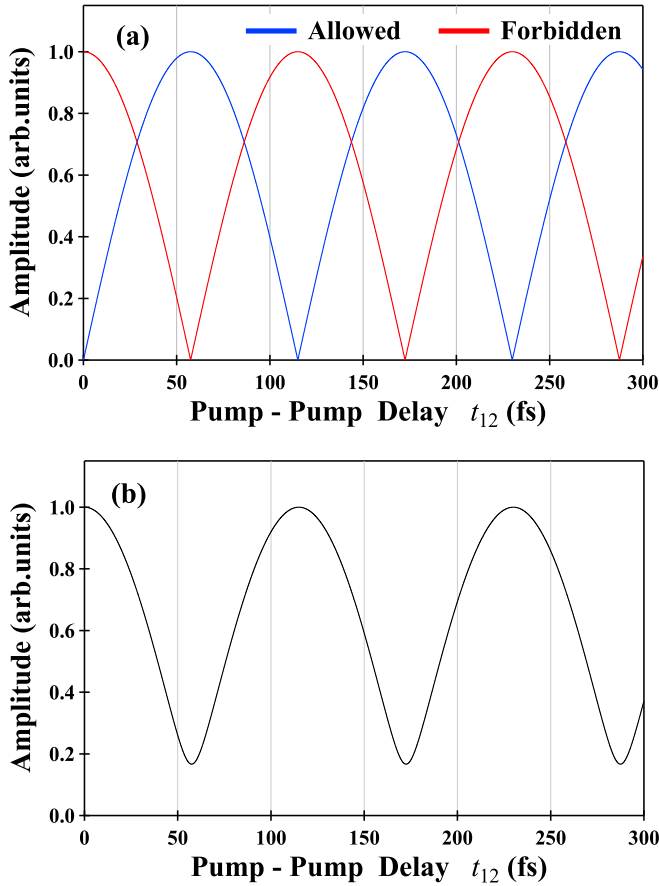


FIG. 5. Amplitude of the LO phonons induced by the orthogonally polarized pulses ($\varphi = \pi/2$ and $\theta = \pi/4$) as a function of the delay t_{12} . (a) The red and blue curves show the amplitude of phonons induced by the allowed and forbidden Raman scattering, respectively. (b) Phonons induced via the total Raman tensor with $\beta/\alpha = 6$. The vertical axis is normalized such that the maximum value is 1.

1. At the $\theta = \pi/4$ orientation

Setting $\varphi = \pi/2$ and $\theta = \pi/4$ in Eqs (11)–(14), we find

$$\rho_1(t) = (\alpha + \beta)P_{11}(t), \quad (23)$$

$$\rho_2(t) = (-\alpha + \beta)P_{22}(t), \quad (24)$$

$$\rho_3(t) = 0, \quad (25)$$

$$\rho_4(t) = 0. \quad (26)$$

Therefore, only the slow oscillation due to the phonon interference is observed in this geometry. The terms from paths 3 and 4 have opposite signs and their sum becomes zero. Then LO phonons are generated via only paths 1 and 2, and those generated by pulses 1 and 2 interfere constructively for the forbidden Raman term, and destructively for the allowed component at each period of the delay t_{12} , as shown in Fig. 5(a). These features are explained as below.

From Eqs. (21)–(24), the density matrix $\rho(t)$ is obtained as $\rho(t) = \alpha[P_{11}(t) - P_{22}(t)] + \beta[P_{11}(t) + P_{22}(t)]$. Therefore, in the allowed and forbidden Raman scattering, phonons are added and subtracted by pulses 1 and 2, respectively. Thus, the

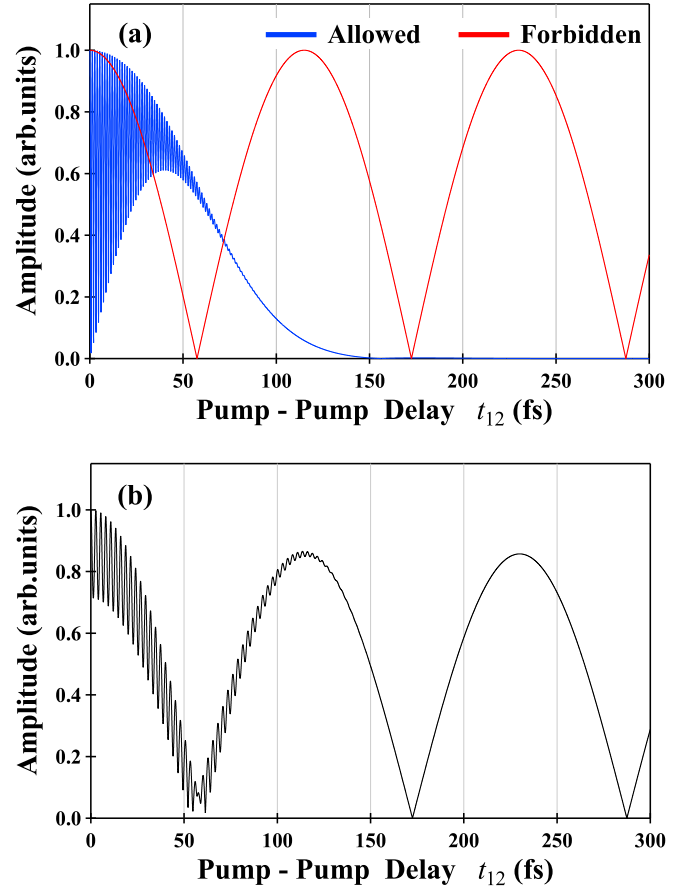


FIG. 6. Amplitude of the LO phonons induced by the orthogonally polarized pulses ($\varphi = \pi/2$ and $\theta = 0$) as a function of the delay t_{12} . (a) The red and blue curves show the amplitude of phonons induced by the allowed and forbidden Raman scattering, respectively. (b) Phonons induced via the total Raman tensor with $\beta/\alpha = 6$. The vertical axis is normalized such that the maximum value is 1.

LO phonons induced by the allowed Raman components by pulses 1 and 2 have opposite phases, such that they interfere destructively at each half-cycle. By contrast, those induced by the forbidden components have the same phase, such that they interfere constructively.

Figure 5(b) shows the LO phonons induced via the total Raman scattering with $\beta/\alpha = 6$. Only the slow oscillation due to the phonon interference is found. An interesting feature is found at $t_{12} = 60$ fs, which corresponds to $t_{12} \cong \pi/\omega$. The phonon amplitude does not decrease to zero in the destructive interference of phonons. This is because of the contribution of the allowed Raman scattering.

2. At the $\theta = 0$ orientation

For $\varphi = \pi/2$ and $\theta = 0$ we find

$$\rho_1(t) = \beta P_{11}(t), \quad (27)$$

$$\rho_2(t) = \beta P_{22}(t), \quad (28)$$

$$\rho_3(t) = \alpha P_{12}, \quad (29)$$

$$\rho_4(t) = \alpha P_{21}. \quad (30)$$

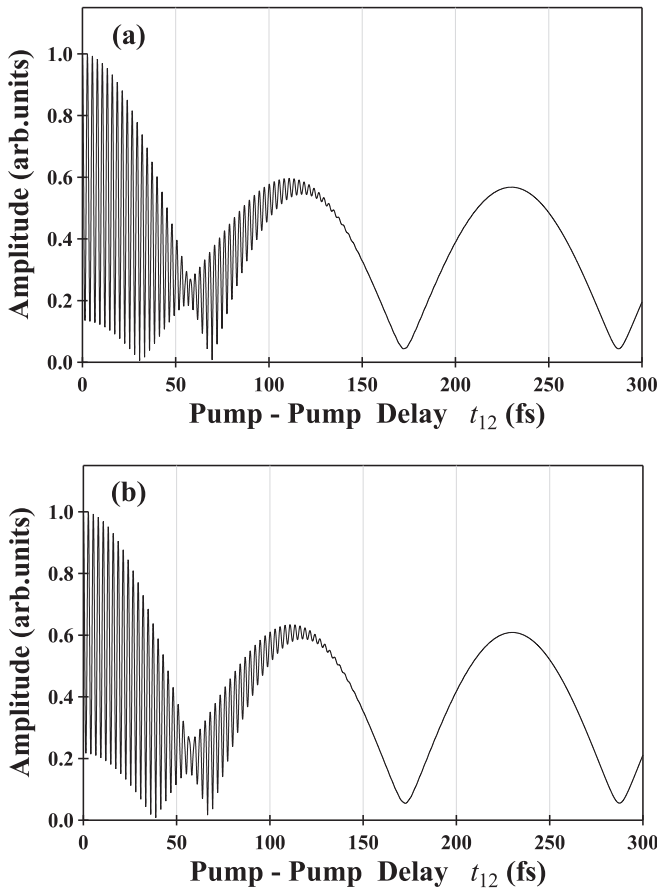


FIG. 7. Amplitude of LO phonons induced by pulses with a relative polarization angle of $\pi/4$ with (a) $\theta = 0$ and (b) $\theta = \pi/2$. The vertical axis is normalized such that the maximum value is 1.

In this geometry, only phonon interference is induced by the forbidden Raman scattering, and electronic interference is induced by the allowed scattering on paths 3 and 4, as shown in Fig. 6. The amplitude of the LO phonons induced via forbidden Raman scattering at $\theta = 0$ is the same as that at $\theta = \pi/4$. By contrast, the amplitude of the LO phonons induced via the allowed Raman scattering shows interference fringes with fast oscillation at a frequency of $2\Omega_0$ owing to electronic interference during the overlap between pulses. Figure 6(b) shows the amplitude of the LO phonons induced via both the allowed and forbidden Raman scattering with $\beta/\alpha = 6$. The interference fringes have a fast oscillation with a frequency of Ω_0 . However, the superposition of the results from each Raman tensor is different from the interference fringes in Fig. 6(b), because there is no contribution from the cross terms due to the quantum-path interference. Furthermore, Figs. 6(a) and 6(b) show the difference of the rapidly oscillating electronic interference fringes. These oscillate at $2\Omega_0$ for allowed Raman scattering only [Fig. 6(a)] and at Ω_0 for both allowed and forbidden scattering [Fig. 6(b)]. These features can be explained as below.

In the condition ($\varphi = \pi/2, \theta = 0$), the allowed Raman scattering [Fig. 6(a)] generates LO phonons via paths 3 and 4. Paths 3 and 4 induce factors of $\exp(-i\Omega_0 t_{12})$ and $\exp(i\Omega_0 t_{12})$, respectively.

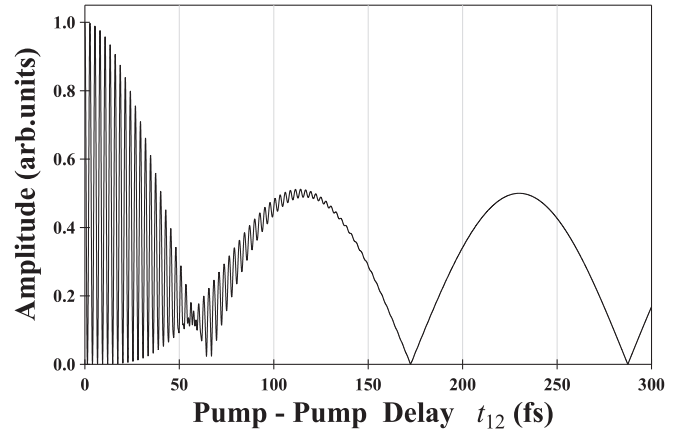


FIG. 8. Phonon amplitude as a function of t_{12} for the space-charge model. The dephasing rate Γ is set to be 0.03 eV. The vertical axis is normalized such that the maximum value is 1.

When the double pulses overlap at $t_{12} \sim 0$, the phonon amplitude is roughly proportional to $|\exp(-i\Omega_0 t_{12}) + \exp(i\Omega_0 t_{12})|$, resulting in the $2\Omega_0$ oscillation. As the delay time increases, the contribution of path 4 decreases rapidly, so that the rapid oscillation disappears. By contrast, the coexistence of allowed and forbidden Raman scattering induces phonon interference via paths 1 and 2. The contribution for the slow oscillation is treated as a constant (e.g., denoted as A). The absolute value of the sum $|A + \exp(-i\Omega_0 t_{12}) + \exp(i\Omega_0 t_{12})|$ causes the dominant Ω_0 oscillation because the value of A (the contribution of the β term) is much larger than unity by assumption.

C. Pulses with a relative polarization angle of $\pi/4$ ($\varphi = \pi/4$)

Figure 7 shows the calculated amplitude of LO phonons with $\beta/\alpha = 6$ for pulses with a relative polarization angle of $\pi/4$ as a function of the pulse delay t_{12} . The electronic and phonon interference fringes are found at $\theta = 0$ and $\theta = \pi/2$. In contrast with the parallel-polarized pulses, the fringe pattern is slightly dependent on θ . For example, the amplitude of the electronic interference at $t_{12} \approx 50$ fs for $\theta = \pi/2$ is larger than that at $\theta = 0$. The interference fringes in this polarization condition can be understood as the superposition of interference by the parallel- and orthogonally polarized pulses.

In the model we used the single-electron approximation. This might be reasonable for the ISRS process and the calculated results well represent the experimental results for the parallel condition [27]. The multielectron effects, for example the relaxation by electron-electron interactions, might be considered for an absorption process.

D. Case of the mechanism with space-charge field

Figure 8 shows the amplitude of the coherent phonons generated by the double pulse with parallelly polarized-pulse excitation via the suppression of the space-charge field as a function of the pump-pump delay (t_{12}). The dephasing rate Γ was set to be 0.03 eV. The interference fringe with a period of 2.7 fs also shows a collapse and revival feature as that via the ISRS process with a large β . However, the amplitude of the

phonons at timing when the electronic interference collapse (approximately 60 fs) is smaller than that via the ISRS process. The interference fringes obtained for the space-charge fields with $\Gamma = 0.03$ eV is similar to that for the ISRS with $\Gamma = 0.06$ eV (shown in Appendix B). The polarization dependence of the amplitude of LO phonons are same as that for the large β case for the ISRS process because the electron-phonon interaction is isotropic.

IV. CONCLUSION

We derived a theoretic model for the coherent control of LO phonons in GaAs (001) by relative-phase locked and polarization controlled double-pulse excitation. By considering the impulsive stimulated Raman scattering processes both for the allowed and forbidden transitions, a variety of the interference fringe patterns in the delay-time dependence of the LO phonon amplitude were predicted theoretically. These features are results of the quantum-path interference in the time domain working together with the additional degrees of freedom of the polarization of photons.

In the present work we adopted a model of GaAs as the simplest test material in this subject. Since the Raman scattering in solids is directly related to the microscopic origin of the interactions between the local deformations of solids and the electronic structures, the effect of the optical polarization plays a quite important role in the generation and detection processes of the coherent phonons. This is especially true in the case of coherent phonons in the materials with asymmetric interaction modes, for example bismuth, which has more than two optical phonon modes and electronic states and includes Jahn-Teller interactions [46]. The experimental and theoretical studies of the coherent phonons will be further extended by taking account of the polarization correlation working with the phase-locked double pulse excitation method.

ACKNOWLEDGMENTS

This work was partially supported by JSPS KAKENHI under Grants 15K13377, 16K05396, 17K19051, 17H02797, 19K03696, and 19K22141. We thank Adam Brotchie, Ph.D., from Edanz Group [47] for editing a draft of this manuscript.

APPENDIX A: THE PERTURBATIVE SOLUTION OF THE DENSITY OPERATOR

We show details of the perturbation calculation of the density operator in ISRS process and derivation of Eqs. (16)–(20). In the interaction picture, the time evolution of the electron-phonon couples state $|\psi(t)\rangle$ is given by

$$i\hbar \frac{d}{dt} |\tilde{\psi}(t)\rangle = \tilde{H}_I(t) |\tilde{\psi}(t)\rangle, \quad (\text{A1})$$

in which $|\tilde{\psi}(t)\rangle \equiv \exp[iHt/\hbar] |\psi(t)\rangle$ and $\tilde{H}_I(t) = e^{iH/\hbar} H_I(t) e^{-iH/\hbar}$ with a wave function $|\psi(t)\rangle$ in the Schrödinger picture. The equation in Eq. (A1) is formally solved as

$$|\tilde{\psi}(t)\rangle = \exp_+ \left[-\frac{i}{\hbar} \int_{-\infty}^t \tilde{H}_I(\tau) d\tau \right] |\tilde{\psi}(-\infty)\rangle. \quad (\text{A2})$$

The initial state is assumed as $|\tilde{\psi}(-\infty)\rangle = |g, 0\rangle$. We calculated the integral with the second-order perturbative expansion.

The time evolution of the density operator by ISRS is expressed by the double-sided Feynman diagrams (Fig. 2). Here we describe the calculation for the path 1 as an example. For convenience, the excited electronic states are denoted as $|e_1, k\rangle \rightarrow |e_1\rangle$ and $|e_2, k\rangle \rightarrow |e_2\rangle$. In the case of path 1, the photoexcitation and deexcitation processes of the electronic states are caused by pulse 1.

At time t_1 , the dipole interaction with pulse 1 induces photoexcitation process ($|g, 0\rangle \rightarrow |e_1, 0\rangle$), and at time τ , the phonon is created ($|e_1, 0\rangle \rightarrow |e'_1, 1\rangle$) due to electron-phonon interaction. By the interaction, polarization of the electronic state is changed by the terms $|e_x\rangle \langle e_y|$ and $|e_y\rangle \langle e_x|$ or preserved by the terms $|e_x\rangle \langle e_x|$ and $|e_y\rangle \langle e_y|$. At time t_2 , the dipole interaction induces deexcitation process of the electronic state ($|e'_1, 1\rangle \rightarrow |g, 1\rangle$).

Then the density operator $\rho_1(t)$ was obtained as

$$\begin{aligned} \rho_1(t) &= i(\alpha \sin 2\theta + \beta) \sum_k \left(\frac{\mu_k E_0}{\hbar} \right)^2 \omega e^{-i\omega t} \int_{t_1}^{t_2} d\tau \\ &\times \int_{-\infty}^t dt_2 \int_{-\infty}^{t_2} dt_1 f(t_1) f(t_2) e^{-\frac{i}{\hbar}(\epsilon_k - \hbar\Omega_0)(t_2 - t_1)} \\ &\times e^{-\frac{\eta}{\hbar}|t_2 - t_1|} e^{i\omega\tau} |g, 1\rangle \langle g, 0|. \end{aligned} \quad (\text{A3})$$

Since the only term involved in the integration of time τ is $e^{i\omega\tau}$, we calculate $\int_{t_1}^{t_2} e^{i\omega\tau} d\tau$ and get

$$\begin{aligned} \rho_1(t) &= (\alpha \sin 2\theta + \beta) \left(\frac{E_0}{\hbar} \right)^2 e^{-i\omega t} \sum_k |\mu_k|^2 \\ &\times \int_{-\infty}^t dt_2 \int_{-\infty}^{t_2} dt_1 f(t_1) f(t_2) e^{-\frac{i}{\hbar}(\epsilon_k - \hbar\Omega_0)(t_2 - t_1)} \\ &\times e^{-\frac{\eta}{\hbar}|t_2 - t_1|} (e^{i\omega t_2} - e^{i\omega t_1}) |g, 1\rangle \langle g, 0| \\ &= (\alpha \sin 2\theta + \beta) P_{11}(t). \end{aligned} \quad (\text{A4})$$

The term $\alpha \sin 2\theta + \beta$ comes from $\langle e_1 | e'_1 \rangle$:

$$\begin{aligned} \langle e_1 | e'_1 \rangle &= \alpha(\sin \theta \cos \theta + \sin \theta \cos \theta) + \beta(\cos^2 \theta + \sin^2 \theta) \\ &= \alpha \sin 2\theta + \beta. \end{aligned} \quad (\text{A5})$$

At a long time delay t from the pump pulses, the upper limit of the integral can be replaced by ∞ . We performed the integration by substitution with $t_1 = s - u/2$, $t_2 = s + u/2$. Using these parameters, we rewrite the terms $f(t_1)f(t_2)$

and $e^{i\omega t_2} - e^{i\omega t_1}$ as

$$f(t_1)f(t_2) = \frac{1}{\pi\sigma^2\Omega_0^2} \exp\left(-\frac{2s^2}{\sigma^2} - \frac{u^2}{2\sigma^2}\right), \quad (\text{A6})$$

$$e^{i\omega t_2} - e^{i\omega t_1} = 2ie^{i\omega s} \sin\left(\frac{\omega u}{2}\right), \quad (\text{A7})$$

and get the function $P_{11}(t)$ as a function of s and u :

$$\begin{aligned} P_{11}(t) &= 2iAe^{-i\omega t} \sum_k |\mu_k|^2 \int_{-\infty}^{\infty} ds \exp\left(-\frac{2s^2}{\sigma^2}\right) e^{i\omega s} \\ &\times \int_0^{\infty} du \exp\left(-\frac{u^2}{2\sigma^2}\right) e^{-\frac{i}{\hbar}\varepsilon_k u} e^{i\Omega_0 u} e^{-\frac{\gamma}{\hbar}|u|} \\ &\times \sin\left(\frac{\omega u}{2}\right) |g, 1\rangle \langle g, 0|, \end{aligned} \quad (\text{A8})$$

where $A = [E_0/(\sqrt{\pi}\sigma\Omega_0\hbar)]^2$. The integration over s is a Gaussian integral, which gives a common constant $[G = \sqrt{\pi}/2\sigma^2 \exp(-\sigma^2\omega^2/8)]$ for each path. Therefore, we summarize the common constant factor as $B = AG$, which yields the equation

$$\begin{aligned} P_{11}(t) &= Be^{-i\omega t} 2i \int_0^{\infty} du \exp\left(-\frac{u^2}{2\sigma^2}\right) \sin\left(\frac{\omega u}{2}\right) e^{i\Omega_0 u} F(u) \\ &= Be^{-i\omega t} L(0). \end{aligned} \quad (\text{A9})$$

APPENDIX B: Γ DEPENDENCE

We calculated the amplitude of LO phonons with $\beta/\alpha = 6$ for parallel-polarized pulses with $\phi = 0$ and $\theta = 0$ as a function of the pulse delay t_{12} and several Γ values [$\hbar\Gamma = 0.01$, 0.02, and 0.06 (eV)], as shown in Fig. 9. With increasing decay constant Γ , the electronic coherence decreased at a faster rate. The electronic interference fringes show the collapse at time t_c and revival. The amplitude of the LO phonons at t_c decreases with increasing Γ .

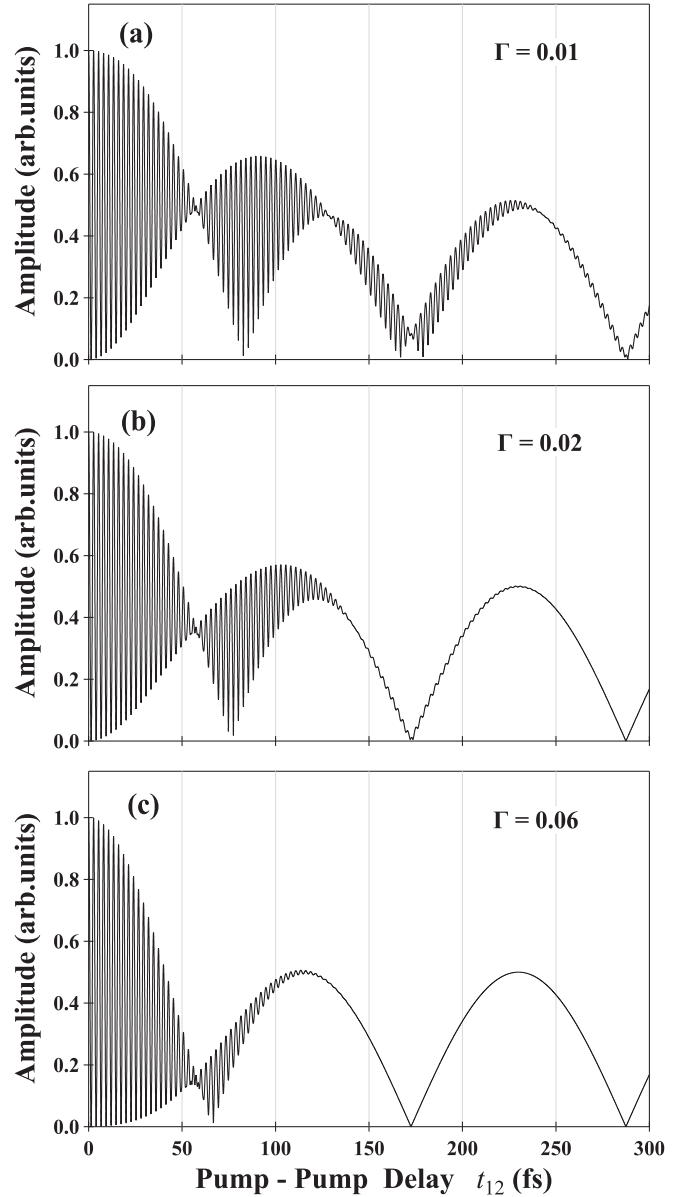


FIG. 9. Amplitude of LO phonons for parallel polarization for different decay constants: (a) $\hbar\Gamma = 0.01$, (b) $\hbar\Gamma = 0.02$, and (c) $\hbar\Gamma = 0.06$ (eV). The vertical axis is normalized such that the maximum value is 1.

- [1] D. J. Tannor and S. A. Rice, *J. Chem. Phys.* **83**, 5013 (1985).
- [2] P. Brumer and M. Shapiro, *Chem. Phys. Lett.* **126**, 541 (1986).
- [3] D. J. Tannor, R. Kosloff, and R. A. Rice, *J. Chem. Phys.* **85**, 5805 (1986).
- [4] D. Meshulach and Y. Silberberg, *Nature (London)* **396**, 239 (1998).
- [5] T. C. Weinacht, J. Ahn, and P. H. Bucksbaum, *Nature (London)* **397**, 233 (1999).
- [6] H. Katsuki, H. Chiba, B. Girard, C. Meier, and K. Ohmori, *Science* **311**, 1589 (2006).
- [7] M. P. A. Branderhorst, P. Londero, P. Wasylczyk, C. Brif, R. L. Kosut, H. Rabitz, and I. A. Walmsley, *Science* **320**, 638 (2008).
- [8] G. Higgins, F. Pokorny, C. Zhang, Q. Bodart, and M. Hennrich, *Phys. Rev. Lett.* **119**, 220501 (2017).
- [9] M. U. Wehner, M. H. Ulm, D. S. Chemla, and M. Wegener, *Phys. Rev. Lett.* **80**, 1992 (1998).
- [10] M. V. Gurudev Dutt, L. Childress, L. Jiang, E. Togan, J. Maze, F. Jelezko, A. S. Zibrov, P. R. Hemmer, and M. Lukin, *Science* **316**, 1312 (2007).
- [11] D. Press, T. D. Ladd, B. Zhang, and Y. Yamamoto, *Nature (London)* **456**, 218 (2008).
- [12] H. Katsuki, Y. Kayanuma, and K. Ohmori, *Phys. Rev. B* **88**, 014507 (2013).
- [13] H. Tahara and Y. Kanemitsu, *Phys. Rev. B* **90**, 245203 (2014).

- [14] B. Pingault, D.-D. Jarausch, C. Hepp, L. Klintberg, J. N. Becker, M. Markham, C. Becher, and M. Atatüre, *Nat. Commun.* **8**, 15579 (2017).
- [15] H. Mashiko, Y. Chisuga, I. Katayama, K. Oguri, H. Masuda, J. Takeda, and H. Gotoh, *Nat. Commun.* **9**, 1468 (2018).
- [16] Y.-X. Yan, E. B. Gamble, and K. Nelson, *J. Chem. Phys.* **83**, 5391 (1985).
- [17] G. C. Cho, W. Kütt, and H. Kurz, *Phys. Rev. Lett.* **65**, 764 (1990).
- [18] H. J. Zeiger, J. Vidal, T. K. Cheng, E. P. Ippen, G. Dresselhaus, and M. S. Dresselhaus, *Phys. Rev. B* **45**, 768 (1992).
- [19] R. Merlin, *Solid State Commun.* **102**, 207 (1997).
- [20] T. Dekorsy, G. C. Cho, and H. Kurz, in *Light Scattering in Solids III*, edited by M. Cardona and G. Güntherodt (Springer, Berlin, 2000), pp. 169–209.
- [21] K. G. Nakamura, Y. Shikano, and Y. Kayanuma, *Phys. Rev. B* **92**, 144304 (2015).
- [22] A. M. Weiner, D. E. Leaird, G. P. Wiederrecht, and K. A. Nelson, *J. Opt. Soc. Am. B* **8**, 1264 (1991).
- [23] T. Dekorsy, W. Kütt, T. Pfeifer, and H. Kurz, *Europhys. Lett.* **23**, 223 (1993).
- [24] M. Hase, K. Mizoguchi, H. Harima, S. Nakashima, M. Tani, K. Sakai, and M. Hangyo, *Appl. Phys. Lett.* **69**, 2474 (1996).
- [25] H. Takahashi, K. Kato, H. Nakano, M. Kitajima, K. Ohmori, and K. G. Nakamura, *Solid State Commun.* **149**, 1955 (2009).
- [26] J.-H. Kim, A. R. T. Nugraha, L. G. Booshehri, E. H. Házoz, K. Sato, G. D. Sanders, K.-J. Yee, Y.-S. Lim, C. J. Stanton, R. Saito, and J. Kono, *Chem. Phys.* **413**, 55 (2013).
- [27] K. G. Nakamura, K. Yokota, Y. Okuda, R. Kase, T. Kitashima, Y. Mishima, Y. Shikano, and Y. Kayanuma, *Phys. Rev. B* **99**, 180301(R) (2019).
- [28] H. Matsumoto, T. Kitashima, T. Maruhashi, I. Takagi, Y. Kayanuma, and K. G. Nakamura, *Solid State Commun.* **327**, 114215 (2021).
- [29] T. Pfeifer, T. Dekorsy, W. Kütt, and H. Kurz, *Appl. Phys. A* **55**, 482 (1992).
- [30] K. Ishioka, A. K. Basak, and H. Petek, *Phys. Rev. B* **84**, 235202 (2011).
- [31] C. Trallero-Giner, A. Cantarero, and M. Cardona, *Phys. Rev. B* **40**, 4030 (1989).
- [32] A. V. Kuznetsov and C. J. Stanton, *Phys. Rev. B* **51**, 7555 (1995).
- [33] T. E. Stevens, J. Kuhl, and R. Merlin, *Phys. Rev. B* **65**, 144304 (2002).
- [34] J. D. Lee and M. Hase, *Phys. Rev. Lett.* **101**, 235501 (2008).
- [35] Y. Shinohara, K. Yabana, Y. Kawashita, J.-I. Iwata, T. Otake, and G. F. Bertsch, *Phys. Rev. B* **82**, 155110 (2010).
- [36] Y. Watanabe, K.-I. Hino, M. Hase, and N. Maeshima, *Phys. Rev. B* **95**, 014301 (2017).
- [37] A. Yamada and K. Yabana, *Phys. Rev. B* **99**, 245103 (2019).
- [38] F. Glerean, S. Marcantoni, G. Sparapassi, A. Blason, M. Esposito, F. Benatti, and D. Fausti, *J. Phys. B: At. Mol. Opt. Phys.* **52**, 145502 (2019).
- [39] T. Kimata, K. Yoda, H. Matsumoto, H. Tanabe, F. Minami, Y. Kayanuma, and K. G. Nakamura, *Phys. Rev. B* **101**, 174301 (2020).
- [40] P. Y. Yu and M. Cardona, *Fundamentals of Semiconductors: Physics and Materials Properties*, 3rd ed. (Springer, Berlin, 2001), pp. 378–394.
- [41] M. D. Sturge, *Phys. Rev.* **127**, 768 (1962).
- [42] H. C. Casey, Jr., D. D. Sell, and K. W. Wecht, *J. Appl. Phys.* **46**, 250 (1974).
- [43] J. I. Kanasaki, H. Tanimura, and K. Tanimura, *Phys. Rev. Lett.* **113**, 237401 (2014).
- [44] A. Alexandrou, V. Berger, and D. Hulin, *Phys. Rev. B* **52**, 4654 (1995).
- [45] J. J. Li, J. Chen, D. A. Reis, S. Fahy, and R. Merlin, *Phys. Rev. Lett.* **110**, 047401 (2013).
- [46] Y. Kayanuma and K. G. Nakamura, *Phys. Rev. B* **95**, 104302 (2017).
- [47] <https://en-author-services.edanz.com/ac>.